

WIND ENERGY SYSTEMS

October 3rd - 6th, 1978

OFFSHORE WIND POWER MODEL ESTIMATES

M. Garstang, R. Pielke,
C. Aspliden, and J.W. Snow

University of Virginia, U.S.A.

Summary

The determination of wind power potential of the coastal wind fields through conversion of wind energy by windmills is examined in terms of a two- and three-dimensional model. The model calculations depend upon land-sea temperature differences, surface roughness changes between land and sea and the large scale thermal and velocity fields. The local land-sea breeze circulation is modified by the synoptic scale flow. A wave-cyclone model is used to provide a preliminary estimate of the frequency distribution of large scale or synoptic conditions on the northeast coast of the United States.

All but one of the two-dimensional model calculations presented show that, at 50 m above the surface, the power density at 5.5 km offshore is more than double that at 5.5 km onshore.

The three-dimensional calculations show that nocturnal stratification results in wind speed maxima migrating out over the water (bay and ocean).

Preliminary analysis of the synoptic scale winds show that for the northeast coast of the United States, storm related conditions dominate during two winter months.

Verification of the model predicted winds is a crucial but incomplete step. Tests of the skill of the model depend upon carefully designed measurements. The potential power of the coastal wind models in predicting optimum locations of wind energy conversion systems in a region of poor observations is great. Application of modeling methods, however, depend upon convincing verification of model predictions.

Held at the Royal Tropical Institute, Amsterdam, Netherlands.

Symposium organised by BHRA Fluid Engineering in conjunction with the Netherlands Energy Research Foundation ECN

©BHRA Fluid Engineering, Cranfield, Bedford, MK43 0AJ, England.

1. Introduction

Many coastal and offshore regions are known in qualitative terms to experience windy conditions. Observations of winds distributed over land and sea across the coastline, however, do not exist in sufficient quality or quantity to provide a clear empirical picture of the coastal and near-shore wind regimes. This is particularly true when detailed interpretations of the low-level coastal wind field must be made to determine the power conversion potential of windmills.

Contrast in land-sea temperature, moisture and consequently atmospheric density fields, on the other hand, results in well known baroclinic regions over and near the coast. The baroclinicity is released on two scales which are of interest to wind power conversion. Diurnal, mesoscale (in the order of 100 km) circulations as well as interdiurnal synoptic-scale (on the order of 1000 km) circulations act in the vicinity of the coastline to convert potential to kinetic energy. Perhaps equally important, these locally intensified circulations result in vertical mixing which transfers the higher velocities of the free atmosphere downward towards the surface. Enhancing this mixing process due to the thermal and moisture fields, is the change in surface roughness from land to sea. Thus, there is ample basis to postulate, on theoretical grounds, that high winds should be encountered over and near many coastlines.

The manner in which the coastal wind circulations are enhanced (or inhibited) will also depend upon the large scale (synoptic) velocity fields and in part upon the effects of the rotating earth (coriolis deflection).

We describe, in this paper, a two- and three-dimensional mesoscale model and the model predicted wind fields on a coastline. Also presented is a preliminary analysis of the frontal-cyclone or synoptic scale influences upon the observed wind fields along the northeast coast of the United States from a wind energy conversion point of view.

2. The Two- and Three-Dimensional Mesoscale Model

The model is developed from first principles of fluid dynamics and thermodynamics incorporating the primitive equation of motion, the energy equation, continuity of mass and a relatively sophisticated parameterization of the boundary layer turbulent fluxes of heat, moisture and momentum. The surface energy balance is computed from the heat balance equation in which short and long wave radiation, latent, sensible and soil heat fluxes are considered. Soil type and soil moisture which influence the heat capacity and conductivity of the soil are included. Aerodynamic roughness is specified over land and calculated over the ocean. The detailed steps of these calculations are set out by Mahrer and Pielke (1).

In the application presented here, the low-level atmospheric circulation in the vicinity of the coastline develops in response to the differential sensible heating and surface roughness between land and sea. The differential heating and roughness interact with the large scale fields of wind and temperature. In the simulation runs, the large scale fields are prescribed from typical conditions or from actual conditions prevailing over the U.S. northeast coast during winter and summer.

The horizontal grid interval is 11 km and 10 km in the two- and three-dimensional calculations, respectively. For the two-dimensional model, calculations were made on a hypothetical north-south orientated coastline with a featureless coastal plain. Calculations were made on a line normal to the shore extending 160 km inland and 160 km offshore. Thus, the two-dimensionality is in terms of the x (coast normal) and z (vertical) coordinates. For the three-dimensional model a rectangular grid of 250 by 360 km was placed over the Chesapeake Bay for featureless terrain. The vertical resolution in the 2-D model is 3 m over 17 levels up to 51 m, while that chosen in the 3-D model calculates winds at 11 levels, 3 m to 48 m at 9 m intervals, followed by the 100, 500, 1000, 2000, and 3000 m levels. In the 3-D model 10 layers were used in the soil with a constant spacing of 5 cm.

The time step of the integration for both models was 60 sec, with the 2-D model run over 10-12 hours following sunrise while the 3-D model is run in over a 24 hour calculation which begins at sunset. The calculations were made primarily on the CRAY computer at the National Center for Atmospheric Research in Boulder, Colorado.

3. Results of the Two-Dimensional Calculations

In the comparative figures 1 to 7 presented below, distributions of power density (watts/m²) within the first 50 m of the atmosphere from 160 km inland to 160 km seaward of the coastline, for each hour after sunrise are given. The various prescribed conditions are shown in the legend of each figure. The daytime heating of the land is assumed to follow a simple sinusoid which reaches a maximum value 8 hours after sunrise. The amplitude of this variation is prescribed. The large scale temperature field initially (i.e. at sunrise) is uniform and conforms to the U.S. Standard Atmosphere both in surface temperature and in lapse rate (15 C and -6.5 C/km). One comparison is made where the large scale temperature field departs from the U.S. Standard Atmosphere. The large scale wind field, is in all cases prescribed as either coast-normal or coast parallel; U_g is the coast-normal geostrophic wind, V_g the coast-parallel geostrophic wind. Latitude, which affects Coriolis turning, is either 30°N or 40°N. The surface roughness length of the land is 4.0 cm in all cases except the last comparison where it is increased to 40.0 cm.

The wind vector at 50 m, located at the first grid point offshore (5.5 km from the coastline) is plotted immediately to the right of each hourly power distribution. Isolines of power density are drawn on each distribution to depict the general field of power density. Power density maxima are identified by heavy dots and the values for each one of these is listed to the right of the distributions.

Comparison #1 (Fig. 1) shows the difference in the daytime development of coastal wind power resulting from an offshore ($U_g > 0$) versus onshore ($U_g < 0$) large scale wind field. All other prescribed values are alike. As the daytime progresses, the power density close to and over the land increases under both conditions. This essentially afternoon power density maximum is common to all situations shown and results from the local wind field increasing in response to the daytime development of a relatively strong horizontal temperature gradient. However, the primary point to note in this first comparison is the location of the maximum power density. With offshore large scale flow and an increasing onshore sea breeze the power density maximum remains in a nearly fixed location, between 5 and 10 km offshore throughout the daytime. In contrast, with onshore large scale flow and the increasing landward component of the sea breeze, the primary power density maximum is carried progressively inland during the afternoon to a location nearly 100 km from the coastline by sunset. A secondary maximum, however, remains just offshore.

The second comparison illustrates the effect of doubling the large scale offshore wind. The nearly stationary power density maximum is preserved and a more than 100% increase in the intensity of that maximum is realized, particularly during the late afternoon. Further strengthening of the offshore geostrophic wind to 15 m/sec (not shown) likewise shows a substantial power density increase but the maximum was displaced seaward nearly 50 km.

The effect of doubling the onshore geostrophic flow is illustrated in Comparison #3. The inland propagation of the primary power density maximum is preserved but the substantial increases in its intensity, realized with the same increase in an offshore large scale wind, is not found. However, an integration over the whole vertical transect of the coastal zone shows that total power is similar for both the doubled onshore and offshore flows. But in the onshore case there is not a well concentrated center of high power density. In essence, the horizontal temperature gradient tends to be more diffused when moderate large scale wind and the sea breeze act in the same direction. A weak secondary power maximum remains just offshore.

Comparison #4 shows the effect of a southerly versus northerly large scale flow. The geostrophic winds are coast parallel, and are of the same light intensity, 5 m/sec,

but are from opposite directions. The southerly geostrophic wind results in a power density distribution quite similar to Comparison #1, the offshore case. This is reasonable since Coriolis in our hemisphere tends to turn a wind from the south into a wind from the west, i.e. offshore. And likewise, with light geostrophic wind from the north, the development resembles the onshore case of Comparison #1. In this case, however, the concentration of power density is reduced as are the magnitudes of any maxima.

In all 4 of the comparisons examined so far, a persistent, although not always primary, power density maximum resides just off the coast.

Comparison #5 tests the effect of a 10° latitude change in the Coriolis turning, specifically 30°N versus 40°N . The geostrophic flow is onshore in both of these cases. Little effect other than the primary power-density maximum occurring 10 to 15 km further inland at 30°N than at 40°N is seen.

The 6th comparison involves changes in the diurnal variation of surface temperature and in the atmospheric lapse rate, i.e. in its stratification. These changes simulate winter versus summer conditions along the U.S. east coast. In both cases the large scale flow is light and offshore, specifically $U_g = +5$ mps. Stratification for the wintertime case is -6 C/km, whereas as for the summer it is more stable, -5 C/km. In the wintertime situation the land surface temperature is less than that of the adjacent sea surface; in summer the opposite situation prevails. Without the warmed land surface to decrease the density of the overlying air, no sea breeze develops. A weak and ill-defined power density maximum occurs well offshore due in part to accelerations resulting from the decrease in surface roughness as the air moves from land to sea, and in part to the direction of the low-level temperature gradient being reversed. In contrast, the summer case has the well concentrated and persistent power-density maximum less than 15 km offshore. The development in the summertime state closely resembles the cases shown earlier for light offshore geostrophic flow under the U.S. Standard Atmospheric stratification. However, an important difference is noted for the summertime stratification: power densities as high as 300 watts/m² are consistently found as low as 20 m above the surface just offshore during the afternoon, whereas with U.S. Standard Atmosphere stratification (-6.5 C/km), such power densities are found only above 30 m. The increased stability appears to concentrate the afternoon sea breeze into a more shallow layer.

The final comparison is one of the most interesting. It shows the effect of changing the land surface roughness from 4 cm (tall grass and low bushes) to 40 cm (high bushes up to scrub-pine forest or a built up area). With light offshore geostrophic conditions, the afternoon maximum values within the near-shore zone of high power density are increased by about 50%. Additionally, density values in excess of 300 watts/m² are found at 10 m during most of the afternoon. The increased turbulent transfer of sensible heat over the rougher land results in a more intense and vertically more extensive horizontal temperature gradient, i.e. enhanced baroclinicity during the afternoon.

The following conclusions might be drawn from the 2-D model calculations in the vicinity of an idealized U.S. Atlantic coastline:

- 1) Within the first 15 km offshore a persistent and nearly stationary power density maximum occurs whenever the land is warmer than the adjacent ocean. It is best developed under large scale light to moderate offshore flow but is present under all geostrophic conditions except strong offshore flow, in which case the maximum is present but is displaced well offshore. In Fig. 8, the daytime energy densities i.e. the sum of the power densities for each daylight hour, are presented for each of the 7 comparisons discussed. All energy densities are for an elevation of 50 m. The solid bars are for a location 5.5 km inland, the open bars for 5.5 km offshore. In all cases the energy density offshore is greater; in fact, only in the winter simulation is the offshore value less than double the onshore value.

- 2) Onshore large scale flow results in a primary power density maximum over land which translates inland as the sea breeze develops. Even under such conditions, how-

ever, a secondary maximum occurs just offshore.

3) Latitude has an effect on the diurnal development of coastal winds, but for the range of latitudes found along the U.S. east coast, the effect of a change in latitude on the power density is small.

4) The typical wintertime condition of land surface cooler than adjacent ocean results in diffuse maximum power density located well offshore.

5) The surface roughness of the land portion of the coastal zone is a very sensitive parameter in determining the magnitude and the vertical distribution of power density within the near-shore region. Increased roughness results in increased power density particularly within the lowest 20 m.

4. Results of the Three-Dimensional Calculations

Figure 9 shows the horizontal grid field superimposed upon the complexity of coastline of the Chesapeake Bay and Virginia barrier islands. Coastline orientation and variation in land-water distributions are now taken into consideration. Calculations are carried out for the complete cycle of daytime radiational heating and nighttime radiational cooling.

In the three-dimensional, as opposed to the two-dimensional, model calculations initial atmospheric conditions are observed rather than simulated. Other input (such as soil characteristics) have been simulated. For the example presented in this paper a small but relatively static summertime high dominated the area from sunset on 8 August 1975 through the following day. The geostrophic wind was nearly unchanging, at 330° at 4 m/sec. Additional model initialization for the lower atmosphere was obtained from the 00Z/9 August 1975 radiosonde launched from Dulles International Airport, outside of Washington, D.C. The characteristics of the first 50 cm of soil were taken from the Seventh General Observation Period, Great Plains Turbulence Field Program, 7 September 1953, 1835 CST, O'Neill, Nebraska (Lettau and Davidson, (2)); in which situation conditions were not unlike those in the area of the Chesapeake Bay on 9 August 1975.

The wind speeds within each 10x10 km square in Figure 8, at a height of 48 m above the lower boundary are presented in Table I. Integration was begun at sunset, 8 August 1975, using a time step of 1 minute. Table I shows the horizontal field of wind speed near noon local time. Table II presents a vertical cross section of calculated wind velocities for an east-west transect across the middle of the bay. Wind speeds and directions are shown at 10 km intervals from the surface (3 m) to 3000 m. The inclusion of realistic radiative cooling (and heating) and soil heat transfer processes allows nocturnal cooling to be effectively simulated. This was not possible in the two-dimensional calculations where only daytime heating in the form a simple sinusoidal function was simulated.

Table I shows (with a 330° large scale flow), that nocturnal cooling over the land has resulted in stratification, little vertical mixing and the resultant minimum off the Virginia coast. Over the ocean and over the Bay, sea surface heating maintains vertical mixing and the highest winds, exceeding the initial input speed by nearly 50%, are observed over the open ocean.

In Table II little change in direction is noted. Wind speeds at the location of the transect, dramatize the minimum which has developed as part of the land breeze circulation off the Virginia coast. Here speeds have dropped to below 50 percent of the initial geostrophic value.

Computer techniques have been developed by Mahrer and Pielke (1) which provide graphical presentation of the horizontal and vertical velocity fields. Methods will be evolved to display the velocity in terms of wind power and by integration over the 24 hours to display locations of maximum and minimum power for the climatologically most frequent conditions.

5. Synoptic Scale Controls

The classical open wave frontal cyclone model was used to determine the frequency distributions of the four wave-cyclone sectors: the warm sector, ahead of the warm front, behind the cold front and in the anticyclonic flow separating frontal lows. Table III shows, for two winter months, January and February the frequency of occurrence of each sector and the mean surface wind speeds in each sector.

For the limited sample examined, it appears that stations on the northeast U.S. coast are subject to anticyclonic flow for about half of the time, unstable cold outbreaks about one third of the time and other conditions for the remaining time in the winter months. We believe that analysis of a much larger sample of data will confirm these distributions.

Pronounced thermodynamic instability would be expected for this region in the winter in the sector coincident with and behind the cold front. We note that this occurs nearly one-third of the time in these winter months. Mean winds show an increase of nearly 50% over the other sectors suggesting that the marked instabilities prevailing at or behind the cold front are in fact manifested by higher winds. A significant amount of the mean annual wind power at these coastal stations is, therefore, to be found directly associated with synoptic scale atmospheric events. Calculations of mean annual wind power duration are likewise significantly influenced by this fact. In future work, we will determine how this synoptic scale enhancement couples with the mesoscale circulations to produce the particular wind fields of the coastal regions.

6. Verification

The utility of the model calculations will depend largely upon the skill with which the model predicts the actual wind fields. Careful, quantitative verification of the model results is not yet possible with the available observations. Two qualitative comparisons are presented below, both of which strongly suggest that the model is able to generate the observed wind fields.

In Fig. 10, the model predicted winds at 3 m along the east and west coasts, and at the center of the island of Barbados are reproduced from Mahrer and Pielke (3) and are compared against observations obtained by DeSouza (4) at the equivalent locations. The initial conditions for this experiment corresponded to the climatological mean conditions over the island during the summer. The qualitative agreement between the model predicted and the climatologically observed diurnal variation of the wind at all three sites is good.

The results presented in Figs. 11 and 12 show a comparable experiment over south Florida. In this case, data for a specific day was used as input, although conditions similar to this are observed frequently over the region during the summer. As in the Barbados example, preferred regions of stronger winds occur due to a baroclinicity created by the land-water contrast. In this case a synoptic onshore wind along the east coast has caused the region of strongest gradient (and therefore stronger winds) to move inland during the day (shown in Fig. 11 are the conditions at 1300 EST). Along the west coast, on the other hand, the strongest gradient remained near the coast because the synoptic flow was offshore. Once again there is good qualitative agreement between model predicted and observed wind fields and between the time changes in the calculated and observed wind fields.

The key results indicated by Figs. 10, 11 and 12 are that

- 1) the differential heating between land and water, the large scale wind and temperature structure and the ground characteristics interact to create preferred regions of maximum power. In some cases these regions migrate during the day (such as along the Florida east coast under easterly synoptic flow), while in other situations the regions remain approximately stationary for a large portion of the day (the west coast of Barbados under easterly synoptic flow).

2) In the vicinity of rain and/or deep cumulus systems, local wind circulations and local changes in thermodynamic stability associated with the clouds and precipitation dominate.

7. Concluding Remarks

The coastal region is characterized by distinct dynamic forcing of the wind fields which is reflected in the observations and can be numerically simulated. Because the dynamic forcing of the low-level atmosphere in the vicinity of a coastline is reasonably well understood, it is likely that model predictions of the velocity fields for the purposes of wind power conversion will prove to be particularly useful in this region. The potential of numerical models is most evident in this region of limited data.

Much must be done to determine the skill and limitations of the numerical models. We believe that this can be done by means of highly efficient field experiments. The efficiency of the field test will stem directly from the precision with which objectives of the experiment can be specified through prior knowledge acquired through the numerical model.

Finally, we believe that by determining the dynamics of the wind regimes in the coastal regions we can avoid the pitfalls of blind statistical treatment. In regions where the wind regime is controlled by a variety of scales of motions (mesoscale land-sea breezes and synoptic scale frontal-cyclone) multiple distributions will be present. Traditional statistics cannot be applied without great caution under these conditions. An approach to estimating the potential power to be extracted from the wind which is based upon the knowledge of the driving forces will both make a more accurate assessment of the power available as well as contribute directly to the design of wind generating systems, from the engineering detail of the windmill to the deployment of mills in the field.

Acknowledgements

The work reported here is supported by the U.S. Department of Energy, Wind Conversion Branch, Solar Energy Division through the Richland Office at the Battelle Pacific Northwest Laboratories under contract no. EY-76-S-06-2344. Model computations at the National Center for Atmospheric Research (NCAR) which is supported by the National Science Foundation, were made under a separate award from NCAR. We gratefully acknowledge this support.

References

- (1) Mahrer, Y. and Pielke, R.A.: A numerical study of the air flow over irregular terrain. *Beitrage zur Physik der Atmosphäre*, 50, 98-113. (1977)
- (2) Lettau, H.H. and Davidson, B.: Exploring the atmosphere's first mile, Vol. II, Pergamon Press, New York, New York. (1957)
- (3) Mahrer, Y. and Pielke, R.A.: The numerical simulation of the air flow over Barbados. *Monthly Weather Review*, 104, 1392-1402. (1976)
- (4) DeSouza, R.L.: A study of atmospheric flow over a tropical island. Ph.D. Dissertation, Florida State University, Department of Meteorology, 203 pp. (1972)

Table I. Wind speeds (m/sec times 10) at height 48 m for the Chesapeake Bay area. Prediction for 1700 GMT, 9 August 1975. Values given for each 10x10 km grid square of Figure 9. Outline of coast, thin solid line; land areas stippled. Isotachs at intervals of 1/2 m/sec, bold lines; locations of speed maxima marked by 'X', minima by 'N'. Geostrophic wind for the area 330° at 4 m/sec, direction indicated by slash below table.

		Grid-Square Number																										
		1	2	3	4	5	6	7	8	9	10	11	12	13	14	15	16	17	18	19	20	21	22	23	24	25		
36	39	39	40	40	40	40	40	40	39	38	37	37	39	41	41	40	39	38	38	38	37	37	37	37	37	37	36	36
35	39	39	40	40	40	40	40	40	39	38	37	37	39	41	41	40	39	38	38	38	37	37	37	37	37	37	36	36
34	39	39	40	40	41	41	40	39	38	37	37	38	41	42	41	40	39	38	38	37	37	37	38	38	38	38	37	37
33	39	40	40	40	41	41	40	39	37	36	36	39	42	42	42	40	39	37	36	35	36	36	37	37	38	38	37	37
32	39	39	40	40	41	41	40	38	36	N	37	40	42	42	41	40	39	37	34	32	32	33	34	35	35	35	35	
31	39	39	40	40	41	41	40	38	36	36	38	41	43	42	41	40	38	37	34	31	N	32	33	33	32	32	32	
30	39	39	40	40	41	41	40	38	37	37	40	43	42	41	40	38	38	37	34	32	34	34	34	34	34	34	30	
29	39	39	40	40	41	41	39	38	37	37	40	43	42	41	40	38	38	38	39	37	36	34	34	34	34	34	N	
28	38	39	40	40	41	41	39	37	36	37	41	44	44	42	40	40	38	38	40	42	40	38	32	30	30	30	28	
27	38	39	39	40	41	41	39	37	36	37	40	44	44	42	41	39	39	39	40	43	X	42	38	36	34	34	27	
26	38	38	39	40	42	41	39	37	37	38	42	44	44	42	41	39	39	39	40	42	43	43	41	39	37	37	26	
25	38	38	39	41	42	43	39	37	38	40	43	45	45	43	40	40	39	40	40	41	42	43	42	41	41	41	25	
24	37	38	39	41	41	40	39	38	39	42	44	45	45	42	41	40	40	40	40	40	40	41	42	43	43	43	24	
23	38	38	40	41	41	40	38	37	39	42	43	43	42	41	40	40	40	40	39	39	40	41	43	44	44	44	23	
22	38	39	40	41	41	40	38	37	38	40	40	40	39	39	40	40	40	40	39	37	37	38	40	43	45	45	22	
21	38	39	40	41	42	41	40	38	37	37	36	38	37	38	40	40	40	39	37	38	34	36	39	43	45	45	21	
20	38	39	40	42	42	43	42	40	38	36	N	36	39	41	42	41	40	38	35	33	33	35	40	43	45	45	20	
19	38	39	40	42	43	43	42	41	39	37	37	38	42	44	44	41	39	38	34	33	33	36	40	44	46	46	19	
18	38	39	40	41	42	43	42	41	39	39	39	41	43	44	43	41	39	35	32	32	34	37	42	45	47	47	18	
17	38	39	40	41	42	42	41	40	39	39	40	40	42	42	43	42	39	39	34	31	32	35	39	43	46	47	17	
16	38	39	40	40	41	41	40	38	38	37	38	38	40	42	44	43	38	32	N	33	37	41	45	47	48	48	16	
15	38	38	39	40	40	40	40	39	38	36	36	37	40	45	47	43	35	31	31	35	39	43	46	48	48	48	15	
14	38	38	39	40	40	40	40	40	38	36	36	39	43	48	48	42	35	32	32	37	42	45	48	49	49	49	14	
13	38	38	39	39	40	41	40	40	39	37	38	41	46	X	47	45	35	34	36	40	44	47	49	49	49	49	13	
12	38	38	39	39	40	40	40	40	38	37	38	42	47	49	45	39	35	33	39	42	46	48	50	50	49	49	12	
11	38	38	39	40	40	40	40	40	39	37	38	43	48	48	44	39	36	37	41	44	47	49	50	50	49	49	11	
10	38	39	40	40	41	41	41	40	39	39	40	44	47	46	46	39	38	40	43	46	48	50	50	50	49	49	10	
9	39	39	40	41	41	42	42	41	41	41	42	45	47	46	42	39	40	42	45	47	48	50	51	50	49	49	9	
8	39	40	40	41	42	42	42	42	42	42	42	44	47	49	47	44	42	42	44	47	49	50	51	51	50	49	8	
7	39	40	40	41	42	42	42	43	44	44	45	46	49	51	50	47	46	45	47	48	50	51	51	51	50	49	7	
6	40	40	40	41	41	42	42	43	43	46	46	48	50	X	51	50	49	49	49	50	51	52	52	51	50	49	6	
5	40	40	40	41	41	42	42	43	45	47	48	49	50	50	51	50	51	51	51	52	52	53	52	51	50	49	5	
4	40	40	41	41	41	42	42	43	45	46	47	47	47	47	49	50	52	53	54	54	54	53	52	50	49	4		
3	40	40	41	41	41	42	43	43	44	45	46	46	45	45	47	49	52	54	56	56	56	55	53	51	49	3		
2	40	40	41	41	41	42	43	43	44	45	45	45	44	45	46	49	52	55	57	58	58	56	54	51	49	2		
1	40	40	41	41	41	42	43	43	44	45	45	45	44	44	46	49	52	55	57	58	X	58	56	54	51	49	1	

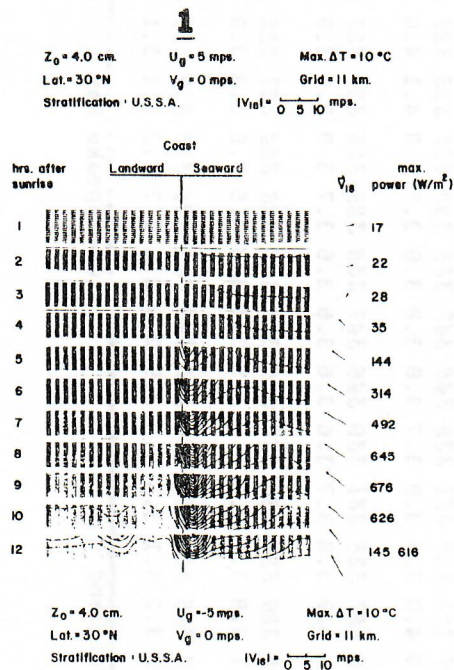
1 2 3 4 5 6 7 8 9 10 11 12 13 14 15 16 17 18 19 20 21 22 23 24 25



Table III. Frequency distribution of frontal cyclones and anticyclone conditions at 10 coastal stations from Cape Hatteras to New Hampshire for the months of January and February 1955

	Warm Sector	Ahead of Warm Front	Behind Cold Front	Anticyclone
Frequency (%)	11.8	6.8	27.1	54.3
Mean wind speed (m sec ⁻¹)	5.6	5.1	7.4	5.0
Standard deviation of the mean (m sec ⁻¹)	2.6	2.2	2.5	1.7

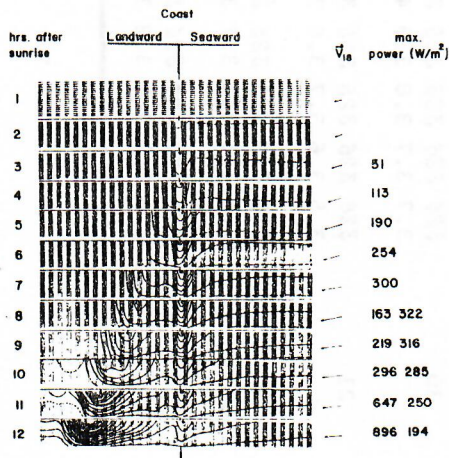
Figures 1 through 7:



Comparisons of model predicted power in watts/m² based on computer output for each hour after sunrise (ordinate) on an 11 km grid (each column) centered on the shore and extending 160 km inland and offshore. The coastline is orientated north-to-south. Each column contains values for heights from 3 to 51 m at 3 m intervals. In the right hand column, maximum power is shown at the location indicated by a dot. The velocity vector at 50 meters for the first grid point offshore (V_{18}) is shown by a scaled arrow. Isolines of power maximum are intended only to show centers of maximum power, values for which appear in the right hand column labelled maximum power (W/m²) corresponding one, two or three centers at that hour. U_g , V_g are west-to-east and south-to-north geostrophic wind components respectively.

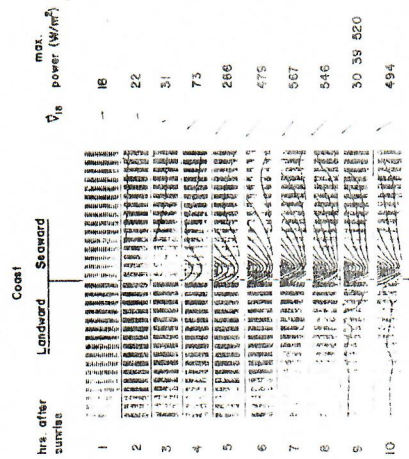
Lapse rates used are:

- USSA: U.S. Standard Atmosphere (-6.5 C/km)
- USWS: U.S. Winter Sounding (-6.1 C/km)
- USSS: U.S. Summer Sounding (-5.0 C/km)

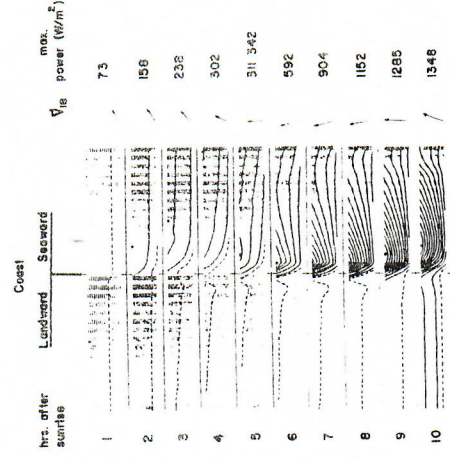


2

Z₀ = 4.0 cm. Max. ΔT = 10 °C
U_g = 5 mps. U_g = 0 mps.
V_g = 0 mps. V_g = 5 mps.
Stratification - U.S.S.A. |V_g| = 0 5 10 mps.

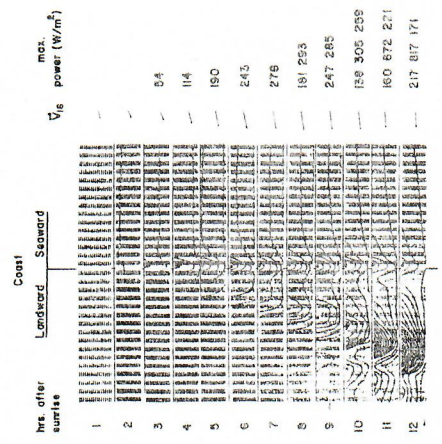


Z₀ = 4.0 cm. Max. ΔT = 10 °C
U_g = 10 mps. U_g = 0 mps.
V_g = 0 mps. V_g = 5 mps.
Stratification - U.S.S.A. |V_g| = 0 5 10 mps.

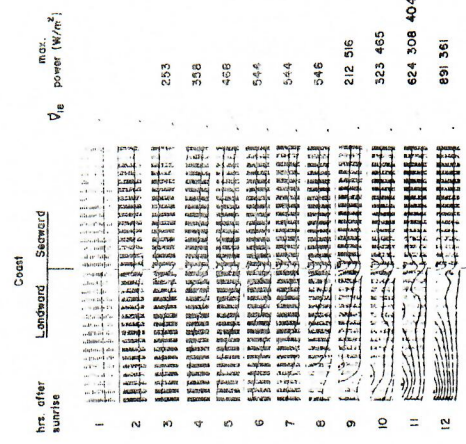


3

Z₀ = 4.0 cm. Max. ΔT = 10 °C
U_g = 5 mps. U_g = 0 mps.
V_g = 0 mps. V_g = 5 mps.
Stratification - U.S.S.A. |V_g| = 0 5 10 mps.

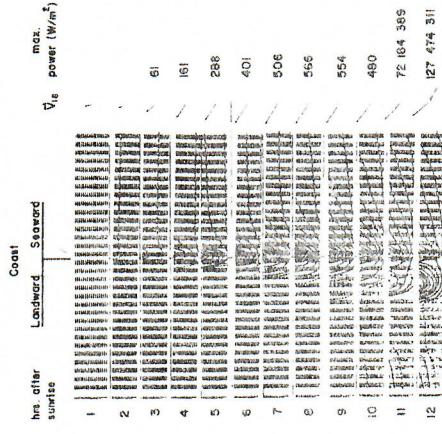


Z₀ = 4.0 cm. Max. ΔT = 10 °C
U_g = 10 mps. U_g = 0 mps.
V_g = 0 mps. V_g = 5 mps.
Stratification - U.S.S.A. |V_g| = 0 5 10 mps.

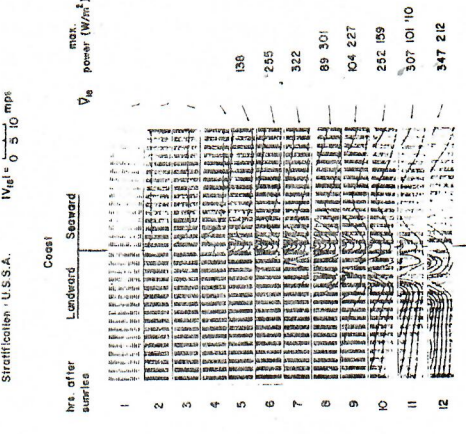


4

Z₀ = 4.0 cm. Max. ΔT = 10 °C
U_g = 0 mps. U_g = 5 mps.
V_g = 5 mps. V_g = 10 mps.
Stratification - U.S.S.A. |V_g| = 0 5 10 mps.

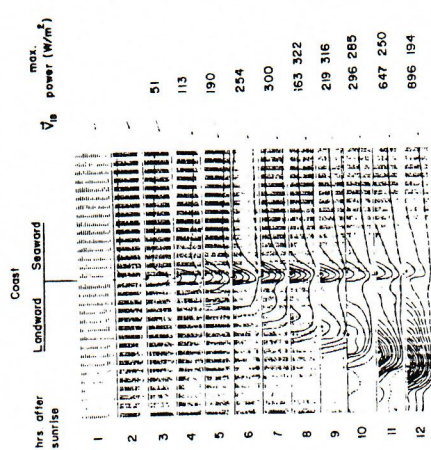


Z₀ = 4.0 cm. Max. ΔT = 10 °C
U_g = 0 mps. U_g = 5 mps.
V_g = 5 mps. V_g = 10 mps.
Stratification - U.S.S.A. |V_g| = 0 5 10 mps.

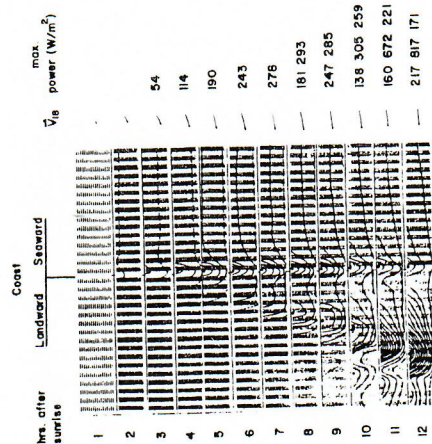


5

Z₀ = 4.0 cm. U_g = 5 mps. Max. ΔT = 10 °C
Lat = 30 °N V_g = 0 mps. Grid = 11 km.
Stratification - U.S.S.A. |V_g| = 0 5 10 mps.

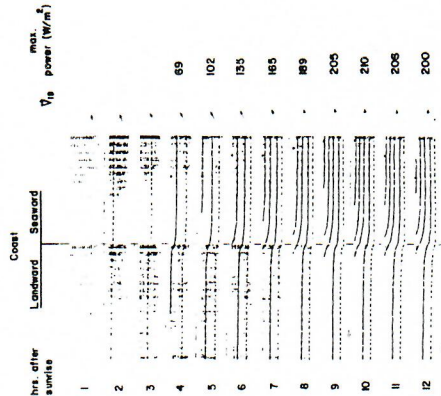


Z₀ = 4.0 cm. U_g = 5 mps. Max. ΔT = 10 °C
Lat = 40 °N V_g = 0 mps. Grid = 11 km.
Stratification - U.S.S.A. |V_g| = 0 5 10 mps.

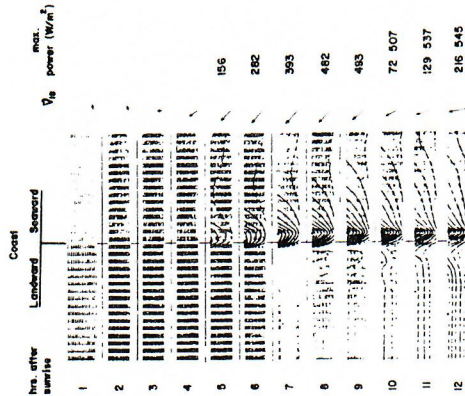


6

Z₀ = 4.0 cm. U_g = 5 mps. Max. ΔT = 10 °C
Lat = 40 °N V_g = 0 mps. Grid = 11 km.
Stratification - U.S.S.A. |V_g| = 0 5 10 mps.

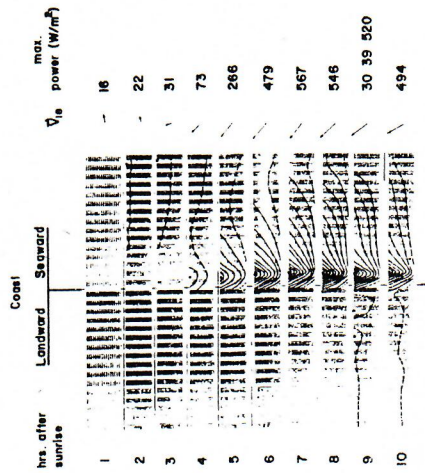


Z₀ = 4.0 cm. U_g = 5 mps. Max. ΔT = 10 °C
Lat = 40 °N V_g = 0 mps. Grid = 11 km.
Stratification - U.S.S.A. |V_g| = 0 5 10 mps.

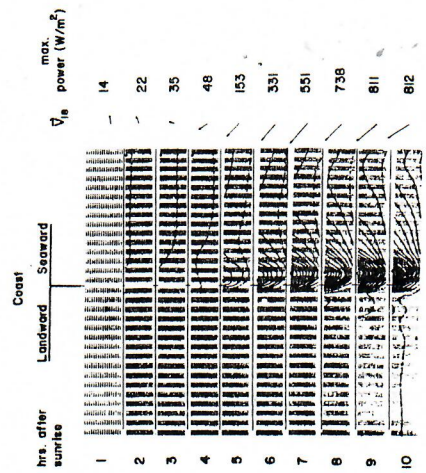


7

Z₀ = 4.0 cm. U_g = 5 mps. Max. ΔT = 10 °C
Lat = 40 °N V_g = 0 mps. Grid = 11 km.
Stratification - U.S.S.A. |V_g| = 0 5 10 mps.



Z₀ = 4.0 cm. U_g = 5 mps. Max. ΔT = 10 °C
Lat = 40 °N V_g = 0 mps. Grid = 11 km.
Stratification - U.S.S.A. |V_g| = 0 5 10 mps.



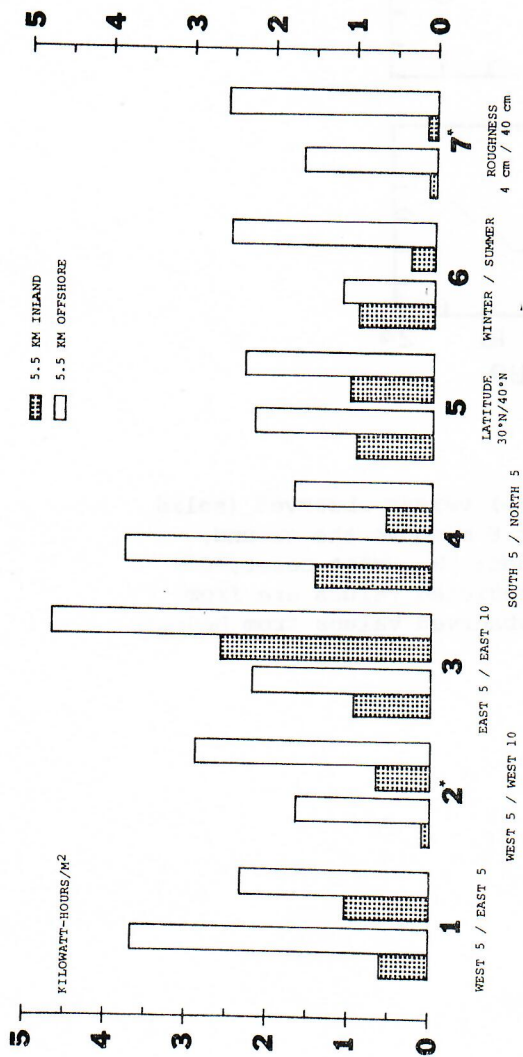


Figure 8: Energy density (kilowatt-hours/m²) for the daylight hours (12 hours unless noted) at 50 m above the surface, 5.5 km inland (stippled bar) versus 5.5 km offshore (open bar). One set of 4 bars for each comparison.

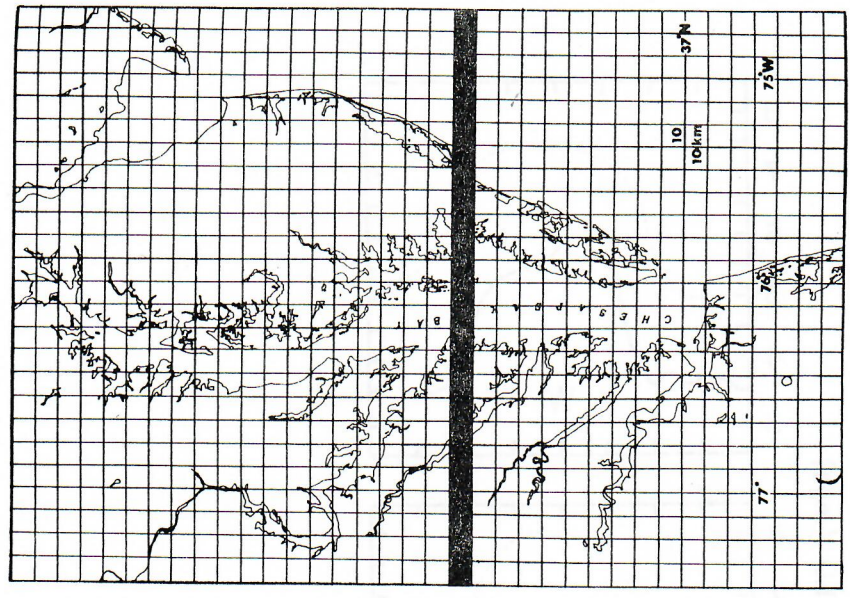


Figure 9:

Ten by ten kilometer grid over 360 x 250 km superimposed upon the Chesapeake Bay and the Atlantic coastline as used in the three-dimensional model. Velocities are calculated for points located at the center of each grid element. The transect used in Table II between grid lines 16 and 17 is indicated by the dark band.

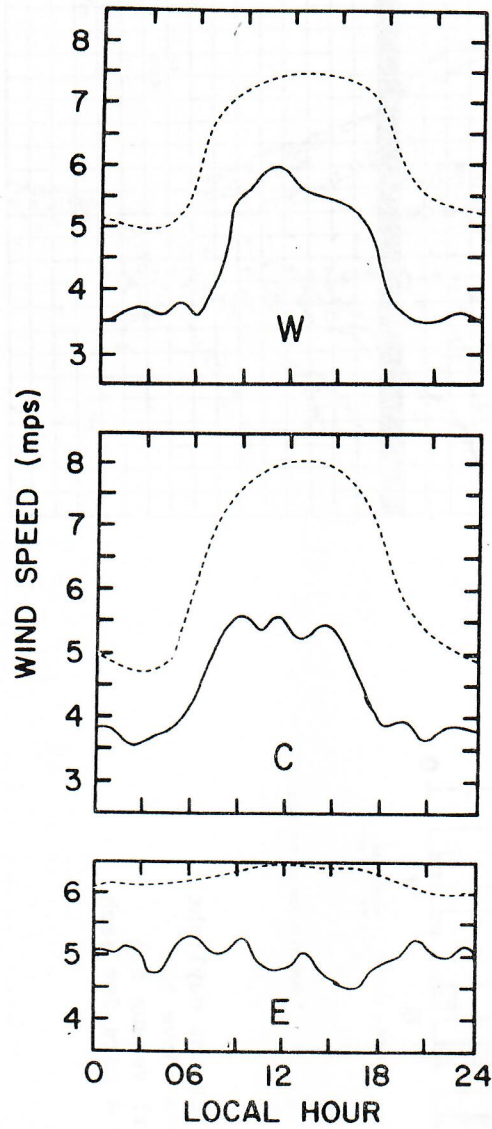


Figure 10: Model-predicted (dashed line) versus observed (solid line) hourly wind speeds at 8 m above the ground, across the island of Barbados: W - west coast, C - center, E - east coast. Predicted values are from Mahrer and Pielke (3) and observed values from DeSouza (4).

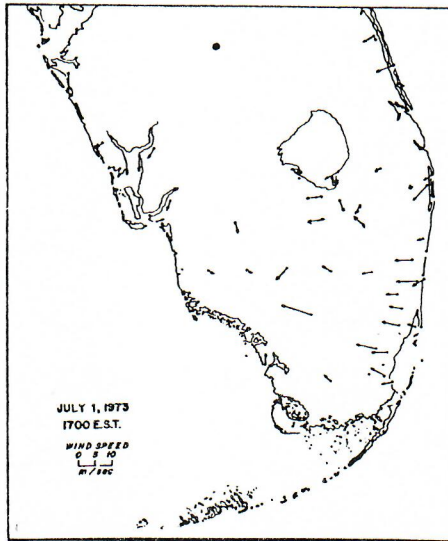
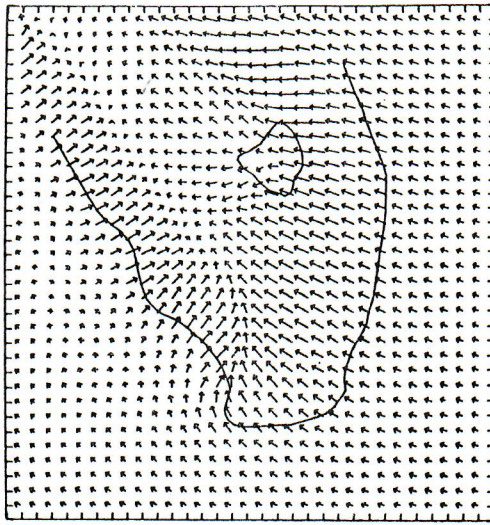


Figure 11: Predicted (upper) and observed (lower) surface winds at 3 m for 1700 EST on July 1, 1973 over the peninsula of Florida. The distance between two marks on the upper figure corresponds to 6 m sec⁻¹.

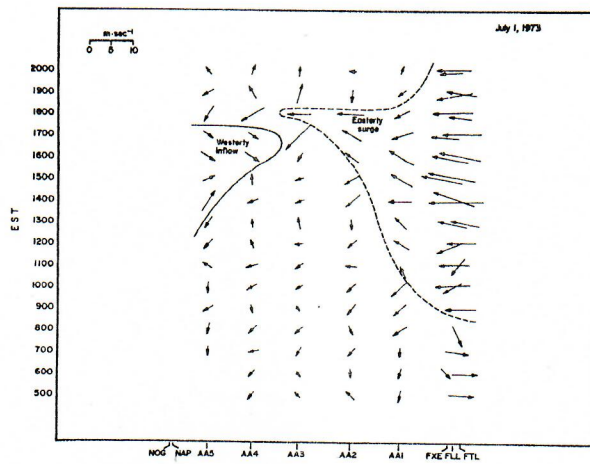
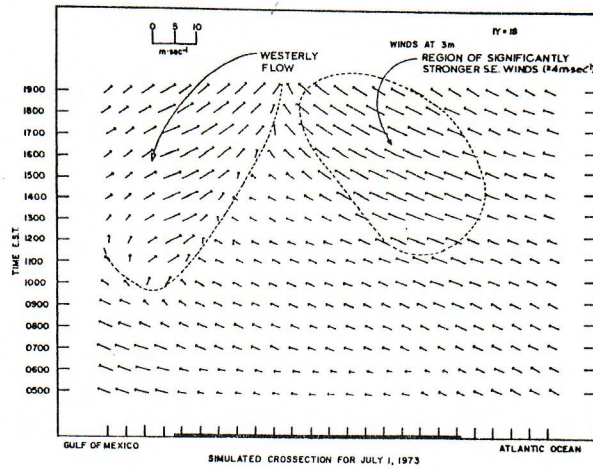


Figure 12: Time cross section of predicted (upper) and observed (lower) surface winds along an east-west line across Florida from Fort Lauderdale to Naples (along the 18th grid line from the southern edge of the model grid).